



https://doi.org/10.1016/j.ultrasmedbio.2022.08.005

Original Contribution

COMPARISON OF ACOUSTOFLUIDIC AND STATIC SYSTEMS FOR ULTRASOUND-MEDIATED MOLECULAR DELIVERY TO T LYMPHOCYTES

CONNOR S. CENTNER,* JOHN T. MOORE,* MARY E. BAXTER,* KAVITHA YADDANAPUDI,

PAULA J. BATES,[‡] and JONATHAN A. KOPECHEK*

* Department of Bioengineering, University of Louisville, Louisville, Kentucky, USA; † Department of Surgery, University of Louisville, Louisville, Louisville, Kentucky, USA; and † School of Medicine, University of Louisville, Louisville, Kentucky, USA

(Received 9 November 2021; revised 22 July 2022; in final form 8 August 2022)

Abstract—Continuous-flow acoustofluidic technologies can potentially improve processing of T lymphocytes for cell therapies by addressing the limitations with viral and non-viral delivery methods. The objective of this study was to assess the intracellular delivery efficiency with acoustofluidic treatment compared with that of static ultrasound treatment. Optimization of parameters in acoustofluidic and static configurations was performed by assessing intracellular delivery of a fluorescent compound (calcein) in viable human Jurkat T lymphocytes. Ultrasound pressure and the concentration of cationic phospholipid-coated microbubbles influenced calcein delivery in both systems. In the static system, a treatment time of 45 s increased molecular delivery compared with 0–30 s (p < 0.01). Refined parameters were used to assess molecular delivery of small and large compounds (0.6-kDa calcein and 150-kDa fluorescein isothiocyanate—dextran, respectively) after ultrasound treatment with the acoustofluidic or static systems. Molecular delivery was similar with refined parameters for acoustofluidic treatment and static treatment (p > 0.05), even though acoustofluidic treatment had lower microbubble concentration (24 μ g/mL vs. 94 μ g/mL) and shorter treatment time (\sim 2–3 s vs. 45 s). This study indicates that the acoustofluidic system can significantly enhance intracellular molecular delivery, which could potentially enable acoustofluidic cell transfection during continuous flow processing for manufacture of cell therapies or other applications. (E-mail: jonathan.kopechek@louisville.edu) © 2022 World Federation for Ultrasound in Medicine & Biology. All rights reserved

Key Words: Acoustofluidics, Sonoporation, Drug delivery, fluorescein isothiocyanate-dextran, T lymphocytes.

INTRODUCTION

Cell-based therapies have the capacity to significantly improve treatment regimens for many diseases, including cancer, autoimmune diseases, infectious diseases and metabolic diseases (Deeks et al. 2002; Brentjens et al. 2007; Buzhor et al. 2014; Schuster et al. 2017; Annesley et al. 2018; Ying et al. 2019). Recent developments in adoptive cell therapies, specifically chimeric antigen receptor (CAR) T cells, have significantly improved patient outcomes in B-cell malignancies, such as leukemia and lymphoma (Annesley et al. 2018). In fact, complete remission rates have been observed in up to 80%–90% of B-cell acute lymphoblastic leukemia patients after treatment in clinical trials (Davila et al.

Address correspondence to: Jonathan A. Kopechek, Department of Bioengineering, University of Louisville, 2301 South Third Street, Lutz Hall, Room 419, Louisville, KY 40292, USA. E-mail: jonathan.kopechek@louisville.edu

2014; Turtle et al. 2016; Gardner et al. 2017). Although similar efficacy has yet to be observed with CAR T treatment for other diseases, there is significant potential to develop improved CAR T and other cell-based therapies, which can enhance targeted cytotoxic activity while reducing off-target effects (Choe et al. 2021). This approach offers a distinct advantage over traditional cancer treatment regimens, such as chemotherapy and radiation, by engineering a patient's own immune cells to directly attack cancer cells. However, limitations with current processing techniques and technologies for CAR T manufacturing, such as genotoxicity caused by viral vectors, have prevented widespread adoption of this biotechnology therapy (Stoiber et al. 2019).

For *ex vivo* modification of T lymphocytes, viral vector technology is primarily being used. Viral vectors have been found to have high efficacy in delivery of nucleic acids to T lymphocytes; however, these results are not reproducible in all cell types because intrinsic

properties of certain cells make it difficult to consistently deliver nucleic acids intracellularly. For example, innate immune cells, such as dendritic cells and macrophages, have evolved to rapidly recognize microbes (e.g., viruses) through pattern recognition receptors, which are able to recognize common components observed in invading microbes (Kawai and Akira 2010). This subsequently triggers downstream pathways to destroy the detected microbes. Limitations with viral vector techniques may include potential insertional mutagenesis, undesired multiplicity of infection and limited nonnucleic acid delivery, such as therapeutic proteins for example. Non-viral transfection approaches have focused on passive loading of human T lymphocytes via physical techniques such as electroporation and shear stress-mediated membrane permeabilization (Sugar and Neumann 1984; Hashimoto and Takemoto 2015; DiTommaso et al. 2018). Static electroporation techniques have generated significant interest as this method uses an applied voltage to induce transient perforation in the plasma membrane and temporally improve intracellular uptake (Sugar and Neumann 1984). However, current electroporation methods have several limitations, including challenges with scale-up for manufacturing processes and generally lower delivery efficacy compared with viral vectors (Naverossadat et al. 2012). For example, one recent study reported more than 95% transduction in HeLa cells using viral delivery (Prel et al. 2015), while another study reported a transfection efficiency of 66% with electroporation (Chicaybam et al. 2016). Recently, a microfluidic squeezing platform has been developed that induces transient perforations in the plasma membrane by taking advantage of the compression forces and the shear stress induced as cells pass through a very narrow constricted channel at a high velocity (Sharei et al. 2013; DiTommaso et al. 2018). The formation of transient perforations enables biomolecules to diffuse from the extracellular buffer into the cytosol (Sharei et al. 2013). However, a fundamental limitation of this technology is the potential for cell debris to cause blockage of the narrow microfluidic channels and prevent consistent processing (Dressaire and Sauret 2016).

To address these limitations, ultrasound technology has the ability to rapidly delivery biomolecules intracellularly using ultrasound contrast agents (*i.e.*, microbubbles) to induce a mechanism known as "sonoporation" (Bhutto et al. 2018; Centner et al. 2020). Sonoporation occurs when ultrasound-induced microbubble cavitation occurs near cell membranes. This phenomenon induces transient perforation of the plasma membrane, which allows intracellular transport of macromolecules that may otherwise be an impermeant because of macromolecular properties such as size, charge and polarity. The

pores in the cell membrane typically repair quickly via active repair mechanisms influenced by factors such as pore size and Ca²⁺ concentration (Zhou et al. 2008; Hu et al. 2013). This approach can potentially enable rapid loading of biomolecules into cells with higher efficacy and viability compared with other physical delivery methods. Microbubbles are currently approved by the U.S. Food and Drug Administration (FDA) for clinical applications involving cardiac imaging, and are also in development for gene therapy and biomolecular delivery applications, including antigenic protein delivery and transfection of immune cells such as dendritic cells and T lymphocytes (Dewitte et al. 2014; Centner et al. 2021a, 2021b). The efficiency of intracellular delivery is a fundamental parameter for effective ex vivo modifications of cells. The coupling of ultrasound and microbubbles potentially offers a solution to address the intracellular delivery limitations of other physical systems. Static ultrasound delivery systems are often used for ultrasound-based molecular delivery systems, which involve single-element transducers or transducer arrays placed in a medium, such as water or cell culture medium, with cells suspended or adhered in a static sample chamber, such as a well plate, petri dish or test tube. However, the volume of these static systems is generally limited by heterogeneous ultrasound pressures outside the ultrasound focus, and throughput is a significant limitation for potential large-scale processing of cell-based therapies. Previously, $500-\mu L$ solutions with 1 min of ultrasound exposure were used for molecular delivery applications (Janis et al. 2021), which enables a maximum processing rate of 30 mL/h.

Acoustofluidic technologies (i.e., coupling of ultrasound and fluidic channels) represent a potential solution to these challenges. Previous studies have determined that acoustofluidics can rapidly enhance intracellular delivery of molecular compounds (Belling et al. 2020; Centner et al. 2020). Some studies have investigated contrast agent-free acoustofluidic methods for molecular delivery applications (Carugo et al. 2011; Longsine-Parker et al. 2013; Belling et al. 2020). Initial studies, however, had limited processing rates (0.1 mL/min) or required coupling of electroporation to induce sufficient transient perforation (Carugo et al. 2011; Longsine-Parker et al. 2013). Recently, contrast agent-free acoustofluidic methods have also induced molecular delivery by utilizing acoustic radiation force to push cells toward the capillary wall coated with a tethered DNA molecule (Belling et al. 2020). Tethering molecules to the capillary wall may not be feasible for some types of biomolecules, and the tethering process may not be compatible with typical aseptic processing methods used for cell therapy manufacturing. We have previously developed acoustofluidic systems that use exogenous microbubbles to enhance molecular delivery to multiple cell types, including cancer cells, erythrocytes and T lymphocytes (Centner et al. 2020, 2021a, 2021b; Janis et al. 2021). This approach has the capacity to process cell solutions with continuous flow rates >100 mL/h, which significantly increases throughput compared with static systems (Centner et al. 2020; Janis et al. 2021). Although acoustofluidics technology has the potential to address limitations of static ultrasound systems for cell processing, the delivery efficiency of each system has not been directly compared.

The objective of this study was to optimize and compare the molecular delivery efficiency using a static ultrasound system and an acoustofluidic system, by modulating microbubble concentration, ultrasound output pressure and ultrasound exposure duration. Although the concepts of sonoporation and ultrasound-mediated molecular delivery are well established, ultrasoundmediated molecular delivery with acoustofluidic systems is not well characterized. In this study, we initially assessed the effect of several key parameters on intracellular delivery efficiency of a fluorescent compound (calcein) in human T lymphocytes. After optimizing key parameters for the static ultrasound system and the acoustofluidic system, we also compared the intracellular delivery efficiency of molecular compounds of different size (0.6-kDa calcein and 150-kDa fluorescein isothiocyanate [FITC]—dextran) after treatment in each system. The molecular weight of 150-kDa FITC-dextran is similar to or larger than those of many proteins (Billett 1990), including clustered regulatory interspaced palindromic repeat (CRISPR) enzymes which can be used for gene editing in CAR T therapy. These results provide new insights into the optimal system and conditions for ultrasound-enhanced molecular delivery of anchorageindependent cells such as T lymphocytes.

METHODS

Molecular delivery to human T lymphocytes

Jurkat T lymphocytes were cultured in RPMI-1640 medium (Cytiva Life Sciences, Marlborough, MA, USA) supplemented with 10% fetal bovine serum (FBS) and 1% penicillin/streptomycin at 37°C and 5% CO₂ in a flat-bottom tissue culture flask. Jurkat T lymphocytes were harvested when 70%-90% confluent and were resuspended in complete RPMI-1640 at a concentration of 100,000 cells/mL after centrifugation at 1500g for 5 min at 4°C. Intracellular delivery of calcein (Sigma-Aldrich, St. Louis, MO, USA) was used to determine optimal parameters in each system for microbubble concentration, ultrasound pressure and ultrasound exposure duration, after ultrasound treatment with an extracellular calcein concentration of 160 µM. Microbubble concentrations between 0 and 94 μ g/mL were tested, as were peak negative ultrasound output pressures between 0 and 5.1 MPa and ultrasound exposure durations up to 60 s. After optimization of microbubble concentration, ultrasound pressure and ultrasound exposure duration for the static system (Fig. 1a) and the acoustofluidic system (Fig. 1b), delivery efficiency was compared by utilizing a small molecule (0.6-kDa calcein) and a large molecule (150-kDa FITC-dextran, Sigma-Aldrich) at a concentration of 1 μ M.

After ultrasound treatment, cells were centrifuged and washed three times with phosphate-buffered solution (PBS) to remove extracellular fluorescent compounds. Flow cytometry (MACSquant, Miltenyi Biotec, Bergisch

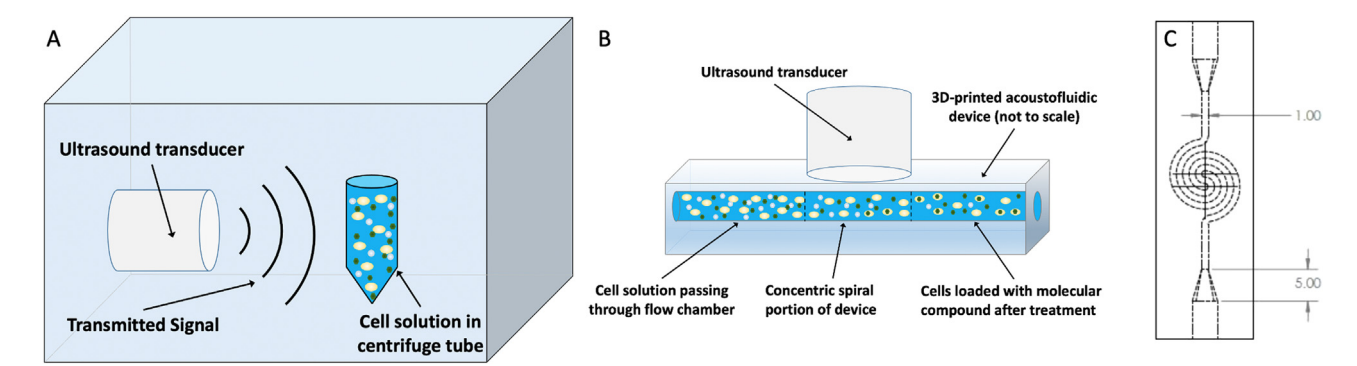


Fig. 1. (a) Static configuration with an ultrasound imaging probe transmitting pulsed ultrasound signal to induce microbubble cavitation in cell solution for enhanced molecular delivery to Jurkat T lymphocytes (not to scale). (b) Acoustofluidic device with an ultrasound imaging probe transmitting pulsed ultrasound signal into the fluidic channel so that microbubble cavitation occurs in cell solution for enhanced molecular delivery to Jurkat T lymphocytes (not to scale). (c) Concentric spiral acoustofluidic device design with 1- × 1-mm channel geometry (not to scale).

Gladbach, Germany) was used to measure intracellular molecular delivery by computing the mean fluorescence intensity after gating out non-viable cells as determined by propidium iodide (PI) staining. On the basis of prior studies, membrane repair typically occurs within min of sonoporation (Fan et al. 2012; Hu et al. 2013; Centner et al. 2021a, 2021b). Therefore, PI was added to samples 30–60 min after ultrasound treatment to ensure sufficient time for membrane repair so that DNA staining was minimized in viable cells. Representative flow cytometry scatterplots in Figure 2 illustrate the gating

procedure after ultrasound treatment. As seen in the scatterplots, propidium iodide fluorescence increases after acoustofluidic treatment (with or without FITC—dextran in these representative samples), which causes a larger number of cells to move into the right-hand quadrants. Furthermore, FITC fluorescence increases after acoustofluidic treatment with FITC—dextran, which causes a larger number of cells to move into the upper quadrants. Cells that stained positive for PI were gated out because of loss of viability, and the mean fluorescence intensity was computed for all viable cells remaining (PI-nega-

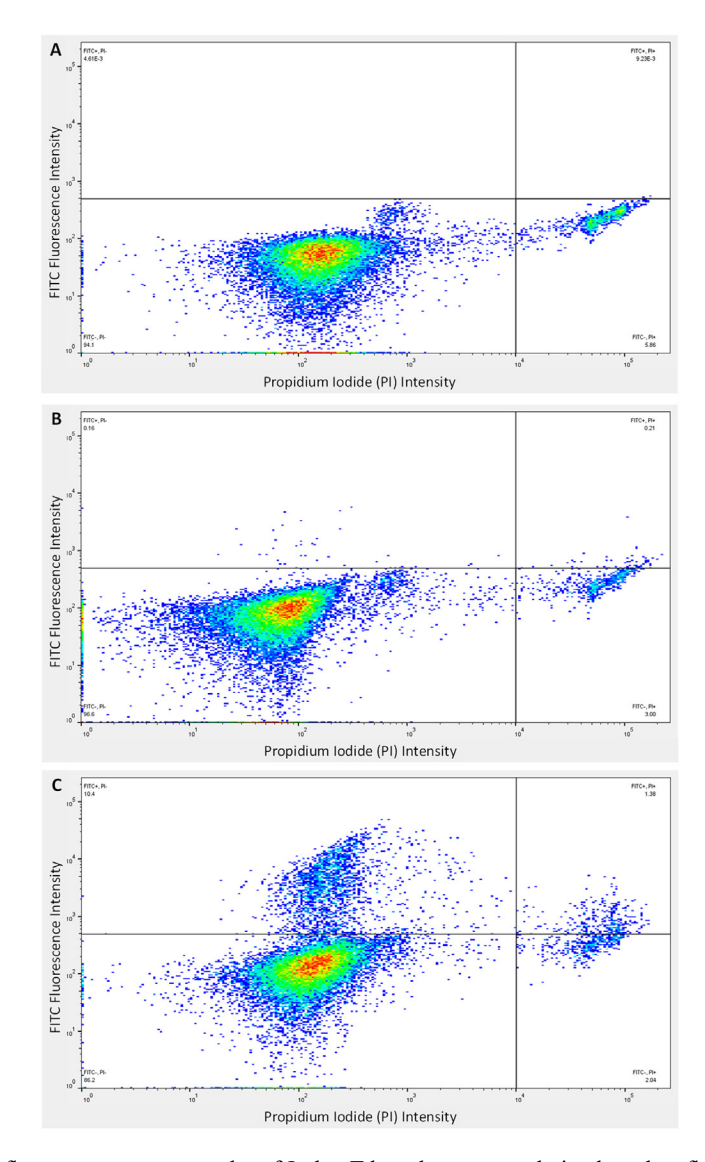


Fig. 2. Representative flow cytometry scatterplot of Jurkat T lymphocyte population based on fluorescein isothiocyanate (FITC) fluorescence intensity and propidium iodide fluorescence intensity. Values in the left-half plane indicate viable cells (PI-) and values in the right-half plane represent non-viable cells (PI+), respectively. (a) Representative flow cytometry scatterplot for a sample with ultrasound treatment and cationic microbubbles in the absence of FITC-dextran. (b) Representative flow cytometry scatterplot for a flow-only control sample exposed to FITC-dextran without ultrasound treatment. (c) Representative flow cytometry scatterplot for a sample exposed to FITC-dextran with acoustofluidic treatment and cationic microbubbles, indicating that FITC fluorescence is significantly increased for viable (PI-) cells.

tive), which were located in the lefthand quadrants of the scatterplots. The FITC gate (between upper and lower quadrants) was not used for fluorescence intensity analysis but is seen in this figure to illustrate the shift in fluorescence above baseline after ultrasound treatment, indicating intracellular delivery of fluorescent compounds in viable T lymphocytes.

Static ultrasound treatment

Static ultrasound treatment was performed in a custom setup as illustrated in Figure 1a, where static refers to the fluid dynamics of the cell solution rather than the dynamic ultrasound wave. This setup was used in previous sonoporation studies (Janis et al. 2021), and is based on similar static sonoporation chambers described in the literature (Miller et al. 1999; Kopechek et al. 2015). Jurkat T lymphocytes (100,000 cells in 1 mL of supplemented RPMI medium) were transferred to 15-mL centrifuge tubes with fluorescent compound (calcein or FITC-dextran) and cationic microbubbles 1 min before ultrasound treatment. The centrifuge tube was placed in a water tank 40 mm away (ultrasound focus) from the P4-1 ultrasound transducer (2.5-MHz center frequency, ATL, Bothell, WA, USA), and B-mode pulses were generated by an ultrasound imaging system (Vantage 64LE, Verasonics, Kirkland, WA, USA) with a pulse repetition frequency (PRF) of 3333 Hz and duty cycle <1%. The free-field ultrasound pressure output was measured using a 0.2-mm needle hydrophone (Precision Acoustics, Dorset, UK) at 40 mm away from P4-1 transducer.

Acoustofluidic treatment

Acoustofluidic treatment was performed in a flow chamber as illustrated in Figure 1b and 1c. The acoustofluidic flow chamber consisted of a concentric spiral channel geometry designed in SolidWorks (Waltham, MA, USA) and fabricated in Accura 60 plastic using stereolithography 3-D printing (Xometry, Gaithersburg, MD, USA) with a cross-sectional channel diameter of 1×1 mm. The concentric spiral design was used to maximize the exposure duration for cells within the ultrasound beam. Stainless-steel barbed tube fittings (10-32 threads, McMaster-Carr, Elmhurst, IL, USA) were inserted into pre-threaded inlet and outlet ports for connection with polyvinyl chloride (PVC) tubing (1/16 in. i. d., McMaster-Carr). Cells were pumped through acoustofluidic channels using a peristaltic pump at a flow rate of 1.5 mL/min (Boxer GmbH, Ottobeuren, Germany), resulting in approximately 2-3 s of ultrasound exposure. A peristaltic pump was used in this study as these are often used for aseptic cell therapy manufacturing processes, but it should be noted that this pump causes pulsatile flow. An ATL P4-1 ultrasound transducer was placed directly on top of the plastic acoustofluidic device with a thin layer of ultrasound gel used for acoustic coupling, and B-mode pulses (2.5 MHz, 12-mm focus, 3333-Hz PRF) were generated by a Verasonics Vantage 64LE ultrasound imaging system. The free-field ultrasound pressure output was measured using a 0.2-mm needle hydrophone (Precision Acoustics) 40 mm away from P4-1 transducer. In situ ultrasound pressures within the acoustofluidic channel could not be measured directly. Current approaches to characterize ultrasound fields within acoustofluidic channels typically use theoretical simulations of the acoustic field or measurements of motile cells that redistribute spatially based on acoustic pressure patterns within the channels (Barnkob and Bruus 2009; Kim et al. 2021). In this study, we reported calibrated free-field output pressure measurements as previously described (Centner et al. 2020, 2021a, 2021b; Janis et al. 2021).

Microbubble synthesis

Cationic microbubbles were synthesized as previously described to form gas-filled microspheres encapsulated by a phospholipid shell (Kopechek et al. 2019). A microbubble formulation with cationic surface charge was used in this study for molecular delivery applications to T lymphocytes, as we previously demonstrated that acoustofluidic treatment with cationic microbubbles significantly enhances molecular delivery compared with a microbubble formulation with a neutral surface charge (Centner et al. 2021a, 2021b). Chloroform soluof 1,2-distearoyl-*sn*-glycero-3-phosphocholine (DSPC, Avanti Lipids, Alabaster, AL, USA), 1,2-distearoyl-sn-glycero-3-ethylphosphocholine (DSEPC, Avanti Lipids), 1,2-distearoyl-sn-glycero-3-phosphoglycerol (DSPG, Avanti Lipids) and polyethylene glycol-40 stearate (Sigma-Aldrich, St. Louis, MO, USA) at a molar ratio of 100:43:1:4.5 were combined in a 20-mL glass vial and desiccated to remove chloroform. An aqueous micellar lipid solution was prepared by adding PBS and sonicating (Qsonica, Newtown, CT, USA) to resuspend the dry lipid film. The resulting 10 mg/mL phospholipid solution was diluted 1:4 in PBS and sealed in a glass vial. The vial head space was filled with decafluorobutane gas (FlouroMed, Round Rock, TX, USA), followed by amalgamation for 45 s at 4350 cpm (DB-338, COXO, Foshan City, China) to form perfluorobutane gas-filled microbubbles (MBs). This synthesis process yields approximately 2×10^9 microbubbles/mL with a mean diameter of $2 \pm 1 \mu m$ determined with a Coulter counter as previously described (Kopechek et al. 2019). A representative brightfield microscopy image of the microbubble solution is provided in Figure 3.

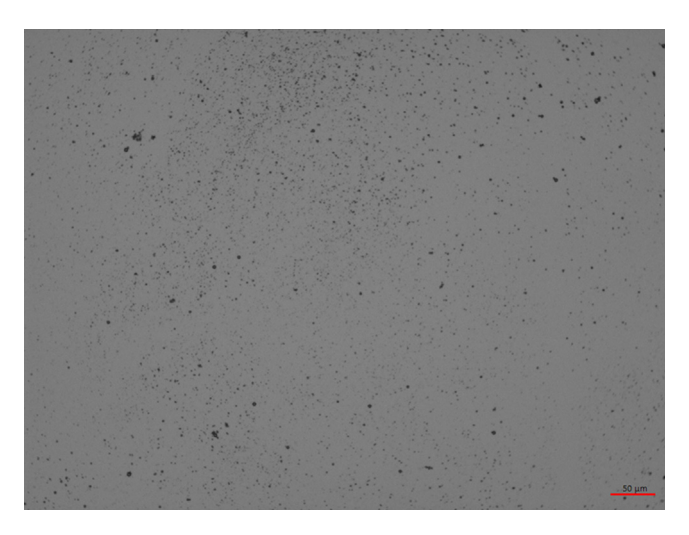


Fig. 3. Representative brightfield microscopy image of cationic microbubbles, which can oscillate in response to ultrasound waves and enhance molecular delivery to nearby cells. Bar = $50 \mu m$.

Microbubble attenuation measurement

Acoustic attenuation measurements of microbubble solutions, which contained 100,000 T lymphocytes/mL in supplemented RPMI medium, were conducted in a separate acoustic chamber as previously described (Centner et al. 2021a, 2021b) to assess the effect of microbubble concentrations, ultrasound treatment pressure and treatment time duration on microbubble destruction in the static and acoustofluidic configurations. A 3-D-printed acoustic chamber was designed in SolidWorks and fabricated using an Ender-3 3D printer (Creality, Shenzhen, China) with a fused filament deposition of 1.75-mm polylactic acid (PLA) filament (McMaster-Carr). Two lead zirconate titanate (PZT) transducers with a center frequency of 3.3 MHz and a diameter of 25 mm (Stem Inc., Davenport, FL, USA) were aligned opposite each other at a distance of 31 mm. The transducers were used as a source and receiver, respectively, to measure acoustic attenuation through each microbubble sample. The microbubble solution was added to 4.5-mL disposable polystyrene cuvettes (VWR, Radnor, PA, USA) with a 1-cm acoustic path length, which were placed in the acoustic chamber at the center of the ultrasound beam. Samples that were tested at different microbubble concentrations were diluted at a 1:4 ratio in 3 mL of PBS to prevent saturation of the acoustic attenuation signal. A waveform generator (DG822, Rigol, Suzhou, China) was used to generate a 3.3-MHz pulse with 500-cycle pulses at an interval of 10 ms. Received ultrasound signals were acquired using a digital oscilloscope (DS1202Z-E, Rigol) at a sampling rate of 10 MHz. All signals were transferred to a desktop computer for processing with MATLAB (The Math-Works, Natick, MA, USA). The attenuation coefficient was calculated using previously described methods (Kopechek et al. 2011). The attenuation coefficient in decibels per centimeter, $\alpha_{\rm dB/cm}$, was calculated where $S_{\rm r}$ and $S_{\rm s}$ are the average power spectrum with and without ultrasound scatter, respectively, and x is the acoustic path distance, measured in centimeters, between the acoustic source and acoustic receiver:

$$\alpha_{\rm dB/cm} = \frac{10 \log(S_{\rm r}/S_{\rm s})}{r} \tag{1}$$

The peak magnitude in the frequency domain was determined at 3.3 MHz for each sample. Without ultrasound, scatter references were acquired with Jurkat T solution containing no microbubbles diluted at a 1:4 ratio in 3 mL of PBS.

Statistical analysis

Statistical analysis was performed using analysis of variance (ANOVA), where statistical significance is defined as p < 0.05, and n represents individual repeats for each experiment. Between-group comparisons were applied by using *post hoc* analysis with Tukey's test. Statistical analysis was performed using SPSS 26 (IBM, Armonk, NY, USA). Bars in figures represent the mean \pm standard error.

RESULTS

Effect of microbubble concentration on intracellular calcein delivery in static ultrasound system

Ultrasound-mediated delivery of calcein to Jurkat T lymphocytes at various microbubble concentrations was evaluated using flow cytometry measurements after ultrasound treatment at an output pressure of 3.8 MPa with an ultrasound exposure time of 30 s. The ultrasound output pressure of 3.8 MPa was previously identified to

be the minimum acoustic pressure required for complete microbubble destruction during acoustofluidic treatment (Centner et al. 2021a, 2021b). Cationic microbubble concentrations between 0 and 94 μ g/mL were tested, and the highest level of molecular delivery occurred after ultrasound treatment at a microbubble concentration of 94 μ g/mL (Fig. 4a, ANOVA p < 0.001, n = 7 or 8/group). Post hoc analysis indicated that intracellular fluorescence was significantly higher after ultrasound treatment at a microbubble concentration of 94 µg/mL compared with 0, 5, 9 or 24 μ g/mL, respectively (p < 0.01). No statistically significant difference in molecular delivery was detected between the 47 and 94 μ g/mL microbubble concentrations (p > 0.05). Measurements of cell membrane integrity using propidium iodide (PI) staining, as an indicator of cell viability, revealed a general decreasing trend at increasing microbubble concentrations (Fig. 4b, ANOVA p < 0.001, n = 7 or 8/group). Cell viability was significantly lower after ultrasound treatment with 94 µg/mL microbubble concentration compared with treatment with 0, 5, 9, 24 or 47 μ g/mL, respectively (p < 0.05), although differences in cell viability between treatment conditions were relatively small and viability remained above 80% after treatment at all microbubble concentrations between 0 and 94 μ g/mL. Acoustic attenuation of each sample was also measured to assess the effect of ultrasound treatment on microbubble destruction at each microbubble concentration. Compared with acoustic attenuation measurements in negative control samples without ultrasound treatment, no statistically significant differences in microbubble destruction were observed at microbubble concentrations of 5, 9 and 24 μ g/mL, respectively (Fig. 4c, ANOVA p > 0.05, n = 6/ group), possibly because of low sensitivity of the acoustic attenuation measurements at these microbubble concentrations. However, significant microbubble destruction was detected after ultrasound treatment at microbubble concentrations of 47 and 94 μ g/mL, respectively (p < 0.001). Intracellular fluorescence intensity levels were highly correlated with levels of microbubble destruction ($R^2 = 0.94$), which suggests that increased microbubble destruction is associated with enhanced intracellular molecular delivery during ultrasound treatment in a static system. Furthermore, cell viability was inversely correlated with microbubble destruction ($R^2 = 0.99$).

Effect of microbubble concentration on intracellular calcein delivery in acoustofluidic device

Intracellular delivery of calcein in Jurkat T lymphocytes was evaluated using flow cytometry after acoustofluidic treatment at various microbubble concentrations. Post hoc analysis indicated that calcein delivery was significantly enhanced after acoustofluidic treatment with the 24 μ g/mL microbubble concentration, compared with all other microbubble concentrations tested with the acoustofluidic system (Fig. 5a, ANOVA p < 0.001, 5 or 6/group). Cell viability was slightly lower after acoustofluidic treatment at the 24 μ g/mL microbubble concentration compared with the negative control group without acoustofluidic treatment or compared with the acoustofluidic treatment at a microbubble concentration of 5 or 9 μ g/mL, respectively (Fig. 5b, ANOVA p <0.001, n = 5 or 6/group), but cell viability remained above 85% after acoustofluidic treatment at all microbubble concentrations tested between 0 and 94 μ g/mL. Acoustic attenuation was very low after acoustofluidic treatment with microbubble concentrations of 5, 9 and

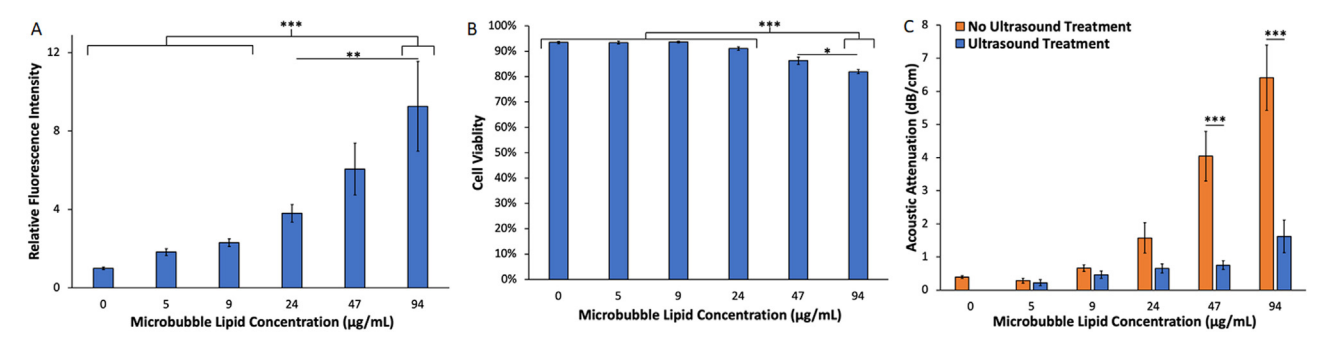


Fig. 4. (a) Delivery efficacy of calcein (100 μ g/mL) with varying microbubble concentrations using static ultrasound treatment (3.8 MPa, 30s). The 94 μ g/mL microbubble concentration enhanced biomolecular delivery of calcein compared with the 0–9 μ g/mL microbubble concentrations (analysis of variance [ANOVA] p < 0.001, n = 7 or 8/group) and 24 μ g/mL microbubble concentration (p < 0.01). (b) The 94 μ g/mL microbubble concentration had reduced viability compared with the 0–24 μ g/mL microbubble concentrations (p < 0.001) and 47 μ g/mL microbubble concentration (p < 0.05), respectively. Cell viability remained >80% for all treatment groups. (c) Acoustic attenuation was significantly reduced for the 47 and 94 μ g/mL microbubble concentrations when treated with ultrasound compared with noultrasound-treatment controls, indicating significant microbubble destruction occurred at these concentrations (ANOVA p < 0.001, n = 6/group).

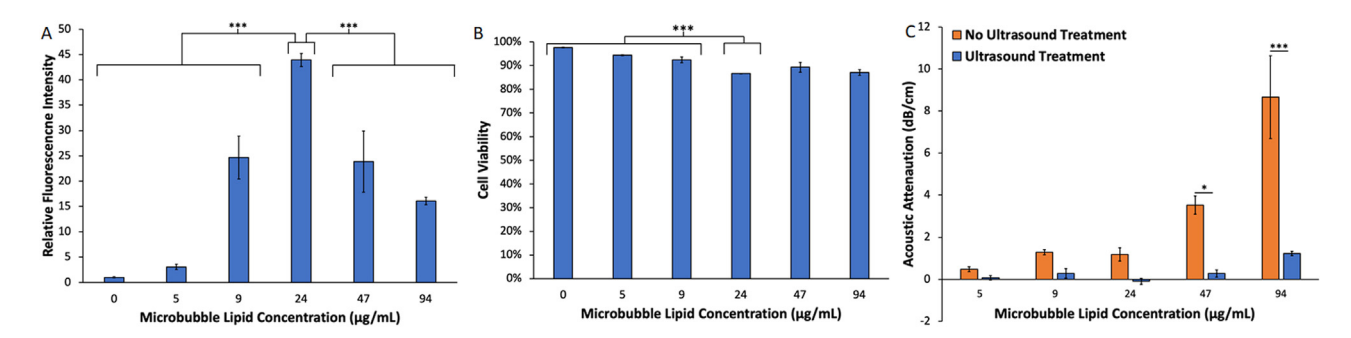


Fig. 5. (a) Delivery efficacy of calcein ($100 \, \mu g/mL$) with varying microbubble concentrations using acoustofluidic treatment (3.8 MPa). The 24 $\mu g/mL$ microbubble concentration enhanced molecular delivery of calcein compared with all other microbubble concentrations (analysis of variance [ANOVA] p < 0.001, n = 5 or 6/group). (b) The 24 $\mu g/mL$ microbubble concentration had decreased viability compared with lower microbubble concentrations ($0-9 \, \mu g/mL$). However, cell viability remained >85% for all treatment groups. (c) Acoustic attenuation was significantly reduced for 47 $\mu g/mL$ (ANOVA p < 0.05, n = 6/group) and 94 $\mu g/mL$ (p < 0.001) microbubble concentrations when treated with ultrasound compared with no-ultrasound-treatment controls, indicating significant microbubble destruction occurred at these concentrations.

24 μ g/mL, although there were no statistically significant differences (Fig. 5c, ANOVA p > 0.05, n = 6/group). Significant microbubble destruction was observed after acoustofluidic treatment at 47 and 94 μ g/mL microbubble concentrations, respectively, compared with measurements at microbubble concentrations of 47 and 94 μ g/mL without ultrasound treatment (p < 0.05 and p < 0.001, respectively). Microbubble destruction was poorly correlated with relative intracellular fluorescence levels ($R^2 = 0.00$), which suggests that increased microbubble destruction is not associated with enhanced molecular delivery based on microbubble concentration in the acoustofluidic system.

Effect of ultrasound output pressure on molecular delivery in static ultrasound system

Molecular delivery was evaluated with flow cytometry after treatment with a static ultrasound system at

various ultrasound pressures for 30 s with a microbubble concentration of 94 μ g/mL. Ultrasound treatment significantly enhanced molecular delivery compared with the negative control group without ultrasound treatment (Fig. 6a, ANOVA p < 0.001, n = 9 or 10/group). Post hoc analysis indicated that there was a statistically significant increase in molecular delivery at a peak negative output pressure of 5.1 MPa compared with no ultrasound (0 MPa) and 2.5-MPa ultrasound pressure output (p <0.001), but no statistically significant differences were detected between ultrasound output pressures of 3.8 and 5.1 MPa (p > 0.05). Flow cytometry analysis of PI staining indicated a general trend of decreasing cell viability with increasing ultrasound output pressure. Post hoc analysis indicated that cell viability after treatment with at an ultrasound output pressure of 5.1 MPa was significantly lower compared with treatment with ultrasound output pressures of 0 MPa (no ultrasound) or 2.5 MPa

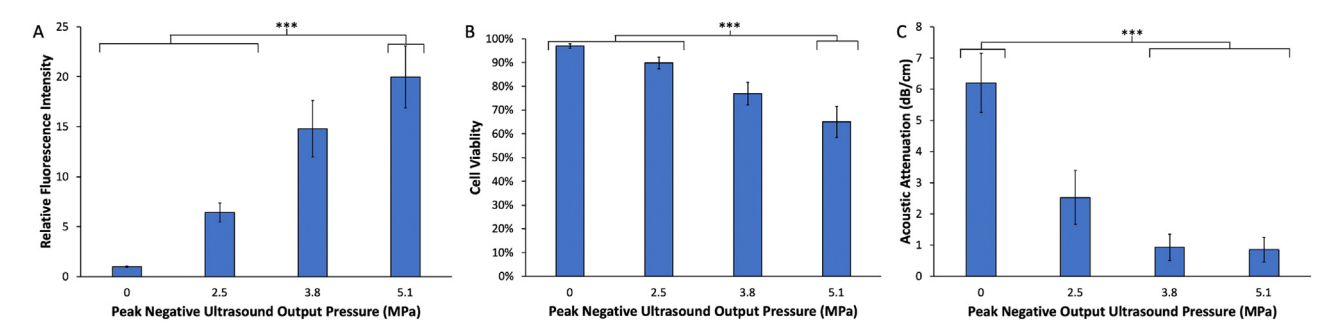


Fig. 6. (a) Static ultrasound treatment (30 s) with the 94 μ g/mL microbubble concentration and varying peak negative output pressure. The 5.1-MPa peak negative pressure enhanced calcein (100 μ g/mL) delivery compared with all other pressures (0 and 2.5 MPa) (analysis of variance [ANOVA] p < 0.001, n = 9 or 10/group). (b) Cell viability remained >65% in all samples. Cationic microbubbles present with and without ultrasound treatment at different treatment pressures. (c) Acoustic attenuation was significantly reduced in samples treated with ultrasound pressures >2.5 MPa (ANOVA p < 0.001, n = 6/group), indicating microbubble destruction at higher acoustic pressures.

(Fig. 6b, ANOVA p < 0.001, n = 9 or 10/group). Although cell viability was reduced with ultrasound treatment, under all treatment conditions, more than 65% of cells remained viable. Acoustic attenuation of each sample was measured to assess the effect of ultrasound output pressure on microbubble destruction during treatment in the static system. A significant decrease in acoustic attenuation was observed with ultrasound treatment compared with no ultrasound treatment (Fig. 6c, ANOVA p < 0.001, n = 6/group). Post hoc analysis indicated that there was a statistically significant difference in attenuation after treatment at ultrasound output pressures of 3.8 and 5.1 MPa compared with no ultrasound treatment (p < 0.001), indicating that higher ultrasound pressures are required for significant levels of microbubble destruction during treatment for 30 s with a microbubble concentration of 94 µg/mL. No statistically significant differences in microbubble destruction were observed between ultrasound output pressures of 3.8 and 5.1 MPa (p > 0.05). Microbubble destruction was highly correlated with relative intracellular fluorescence levels $(R^2 = 0.91)$, which suggests that increased microbubble destruction is associated with enhanced intracellular molecular delivery during ultrasound treatment in a static system.

Effect of ultrasound output pressure on molecular delivery in acoustofluidic system

Acoustofluidic-mediated molecular delivery was evaluated with flow cytometry after treatment at various peak negative ultrasound output pressures between 0 and 5.1 MPa. A significant increase in calcein delivery was detected after ultrasound treatment with the acoustofluidic device, compared with the negative control group that did not undergo ultrasound treatment (Fig. 7a,

ANOVA p < 0.001, n = 6 or 7/group). Post hoc analysis indicated that molecular delivery in the acoustofluidic system was significantly enhanced at ultrasound output pressures of 3.8 and 5.1 MPa compared with 0 MPa (no ultrasound) and 2.5 MPa (p < 0.001). Post hoc analysis also indicated that there was no statistically significant difference in molecular delivery between ultrasound output pressures of 3.8 and 5.1 MPa (p > 0.05). Flow cytometry analysis of PI staining indicated that acoustofluidic treatment reduced cell viability compared with the negative control group without ultrasound (Fig. 7b, ANOVA p < 0.001, n = 6 or 7/group). Treatment with higher ultrasound output pressures (3.8 and 5.1 MPa) caused a statistically significant decrease in viability compared with no ultrasound treatment (0 MPa) and treatment at lower ultrasound output pressures (2.5 MPa, p < 0.001), respectively. However, cell viability remained above 75% viability after acoustofluidic treatment under all treatment conditions (peak negative ultrasound output pressure between 0 and 5.1 MPa). Acoustic attenuation of each sample was measured to assess the effect of acoustofluidic ultrasound pressures on microbubble destruction. No statistically significant differences in microbubble destruction were observed after treatment at ultrasound output pressures of 0 MPa (no ultrasound) or 2.5 MPa (Fig. 7c, ANOVA p > 0.05, n = 4 - 6/group), but there was a significant decrease in acoustic attenuation after acoustofluidic treatment at ultrasound output pressures of 3.8 and 5.1 MPa, compared with the control group without ultrasound. Additionally, acoustic attenuation was higher after acoustofluidic treatment at an ultrasound output pressure of 2.5 MPa compared with treatment at ultrasound output pressures of 3.8 MPa (p < 0.05) and 5.1 MPa (p < 0.01), indicating higher levels of microbubble destruction at

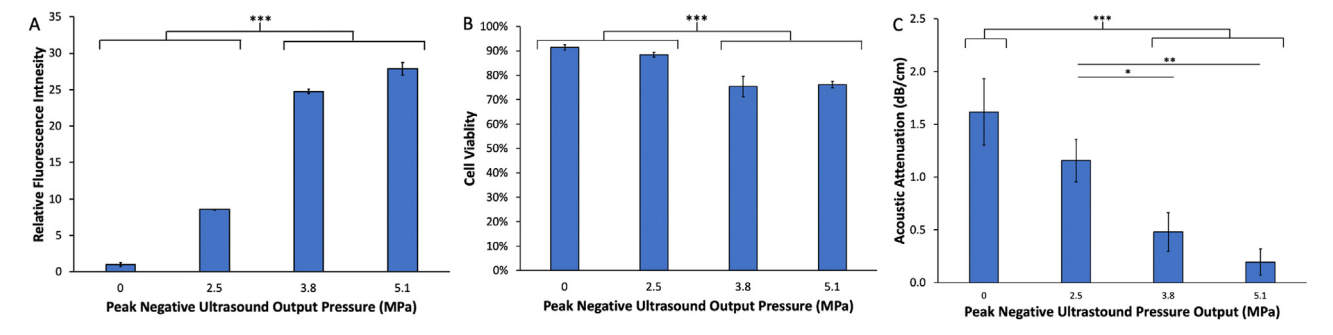


Fig. 7. (a) Efficacy of acoustofluidic device in delivery of calcein ($100 \ \mu g/mL$) with $24 \ \mu g/mL$ microbubble concentration and varying peak negative output pressures; 3.8 and 5.1 MPa enhanced calcein delivery in Jurkat T lymphocytes compared with 0 MPa (no ultrasound treatment) and 2.5 MPa (analysis of variance [ANOVA] p < 0.001, n = 6 or 7/group). (b) Cell viability was reduced in 3.8- and 5.1-MPa treatments compared with 0- and 2.5-MPa treatments, respectively (p < 0.001). Cell viability remained >75% in all samples. (c) Acoustic attenuation was significantly reduced in samples treated with ultrasound pressures >2.5 MPa compared with flow conditions without ultrasound treatment (ANOVA p < 0.001, n = 4 - 6/group). Additionally, 3.8 MPa (p < 0.05) and 5.1 MPa (p < 0.01) had decreased acoustic attenuation compared with 2.5 MPa, indicating microbubble destruction at higher acoustic pressures.

increased ultrasound pressures in the acoustofluidic device. Intracellular fluorescence levels and microbubble destruction were highly correlated ($R^2 = 0.99$), which suggests that increased microbubble destruction is associated with intracellular molecular delivery during acoustofluidic treatment.

Effect of ultrasound treatment time on molecular delivery in static system

The effect of various ultrasound treatment durations between 0 and 60 s was tested with flow cytometry after treatment in the static system at a microbubble concentration of 94 µg/mL. Ultrasound treatment increased molecular delivery compared with the negative control group without ultrasound treatment (0-s treatment duration; Fig. 8a, ANOVA p < 0.001, n = 7 - 9/group). Post hoc analysis indicated that molecular delivery was significantly higher with a 45-s treatment duration than with a 15-s (p < 0.001) or 30-s (p < 0.01) treatment duration, but no statistical difference was detected between 45- and 60-s treatment durations (p > 0.05). Flow cytometry analysis of PI staining indicated a general trend that as treatment time increased, there was a corresponding decrease in cell viability. Post hoc analysis revealed a statistically significant decrease in cell viability after ultrasound treatment compared with the negative control group without ultrasound treatment (Fig. 8b, ANOVA p < 0.01, n = 7 - 9/group), but there were no statistically significant differences in cell viability between ultrasound treatment groups, and cell viability remained at 75% in all treatment conditions (ultrasound treatment durations between 0 and 60 s). Acoustic attenuation of each sample was measured to assess the effect of ultrasound treatment duration in a static system on intracellular molecular delivery. Post hoc analysis indicated that acoustic attenuation was significantly decreased in samples with ultrasound treatment durations ≥ 30 s compared with the negative control group without ultrasound treatment (0 s, Fig. 8c, ANOVA p < 0.01, n = 6 - 12/group), indicating that microbubble destruction persists for more than 15 s during ultrasound treatment. However, no statistically significant differences in acoustic attenuation were detected between ultrasound treatment durations of 30, 45 and 60 s (p > 0.05). A significant correlation was still observed between microbubble destruction and molecular delivery with an R^2 of 0.94, suggesting that increased microbubble destruction is highly correlated with increased molecular delivery.

Effect of ultrasound treatment duration on molecular delivery in acoustofluidic system

The impact of ultrasound treatment duration on calcein delivery to Jurkat T lymphocytes was investigated with flow cytometry after treatment in the acoustofluidic system. Samples were circulated through the acoustofluidic device once or twice (1 x and 2 x ultrasound durations, respectively), with a microbubble concentration of 24 μ g/mL added before each pass through the device) and with (3.8-MPa ultrasound output pressure) or without ultrasound treatment. Exposure time for the acoustofluidic group is approximately 2-3 s per exposure with a flow rate of 100 mL/h. Molecular delivery was significantly higher after $1 \times$ and $2 \times$ ultrasound treatments compared with the respective negative control groups without ultrasound treatment (Fig. 9a, ANOVA p <0.001, n = 6/group). Although the ultrasound treatment duration was double in the $2 \times$ treatment group, post hoc analysis indicated that there was no statistically significant difference in calcein delivery between the two

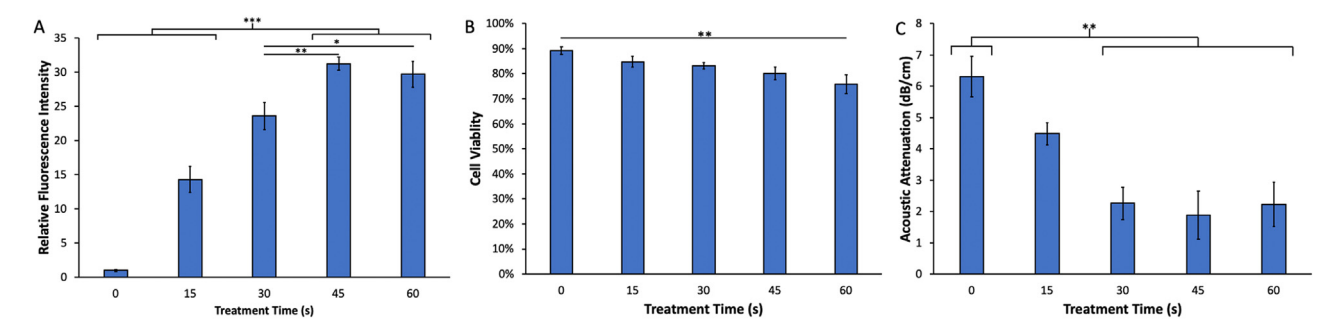


Fig. 8. (a) Delivery efficacy of calcein (100 μ g/mL) with varying treatment times for static ultrasound treatment (5.1 MPa, 94 μ g/mL microbubble concentration). Static ultrasound treatment times of 45 and 60 s enhanced biomolecular delivery of calcein compared with no ultrasound treatment (0 s) and 15 s of static ultrasound treatment time (analysis of variance [ANOVA] p < 0.001, n = 7-9/group). Additionally, 45 s of static ultrasound treatment enhanced calcein delivery compared with 30 s of static ultrasound treatment (p < 0.01). Similar results were observed between 45 and 30 s of ultrasound treatment time (p < 0.05). (b) Cell viability was reduced with 60-s treatment compared with 0-s treatment (no ultrasound, p < 0.01). Cell viability remained a >70% for all treatment groups. (c) Acoustic attenuation was significantly reduced in samples with \geq 30 s of ultrasound treatment time compared with 0 s (ANOVA p < 0.01, n = 6-12/ group).

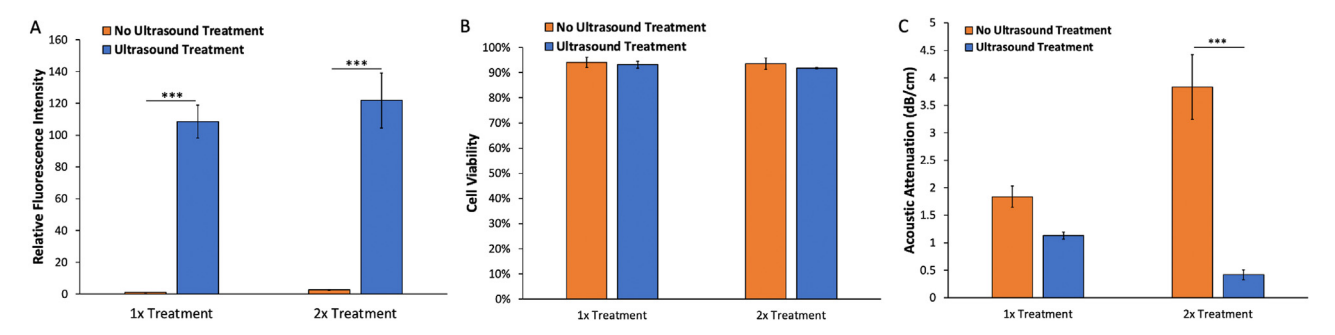


Fig. 9. (a) Delivery efficacy of calcein ($100 \ \mu g/mL$) with varying treatment time for acoustofluidic treatment ($3.8 \ MPa$, $24 \ \mu g/mL$ microbubble concentration). The $1 \times$ and $2 \times$ acoustofluidic treatments enhanced biomolecular delivery of calcein compared with their no ultrasound treatment control, respectively (analysis of variance [ANOVA] p < 0.001, n = 6/group). (b) Cell viability remained >85% for all treatment groups with no statistical significance detected between groups. (c) Acoustic attenuation was significantly reduced in samples with multiple acoustofluidic treatments compared with the multiple flow-only control in which microbubbles were added prior to each treatment (ANOVA p < 0.001, n = 6/group).

ultrasound treatment duration groups, as measured by flow cytometry (p > 0.05). Flow cytometry analysis of PI staining indicated that there were no significant differences in cell viability between ultrasound treatment groups and control groups without ultrasound treatment, and cell viability remained above 85% in each group (Fig. 9b, ANOVA p > 0.05, n = 6/group).

The effect of ultrasound treatment on microbubble destruction was assessed after acoustofluidic treatment. No statistically significant difference in acoustic attenuation was detected between the $1 \times$ ultrasound treatment duration and no ultrasound treatment (Fig. 9c, ANOVA p > 0.05, n = 6/group), but a significant difference in attenuation was measured between the $2 \times$ ultrasound treatment duration and no ultrasound treatment (p < 0.001).

Comparison of refined static and acoustofluidic conditions on intracellular molecular delivery

The efficiency of intracellular molecular delivery in Jurkat T lymphocytes was measured after treatment in the static system and the acoustofluidic system under refined conditions for direct comparison between configurations. Delivery of a small molecule (calcein, 0.6 kDa) and that of a large molecule (FITC-dextran, 150 kDa) were measured for comparison. Static ultrasound treatment and acoustofluidic treatment significantly enhanced molecular delivery of calcein (Fig. 10a, ANOVA p <0.01, n = 5 or 6/group) and 150 kDa FITC-dextran (p <0.001) compared with negative control groups without ultrasound treatment. There was no statistically significant difference in intracellular delivery of calcein or 150-kDa FITC-dextran between static ultrasound treatment and acoustofluidic treatment (p > 0.05), indicating that the acoustofluidic system achieved molecular delivery results similar to those of static ultrasound treatment. Flow cytometry analysis of PI staining indicated that there was a statistically significant decrease in cell viability after treatment with the static ultrasound system (Fig. 10b, ANOVA p < 0.001, n = 5 or 6/group) and acoustofluidic treatment (p < 0.001) compared with negative control groups without ultrasound. However, no statistically significant differences in cell viability were detected between ultrasound configurations (p > 0.05), and cell viability remained >70% after all treatment conditions tested.

Cell viability was also measured using trypan blue assay immediately after treatment (day 0) and 2 d after treatment to assess cell survival and proliferation over time after treatment. As illustrated in Figure 11, the number of viable cells did not statistically differ between acoustofluidic treatment and the flow-only control group immediately after treatment (ANOVA p > 0.05, n = 5/group). At 2 d after treatment, the number of viable cells was higher in the flow-only control group compared with the acoustofluidic treatment group (p < 0.001), but cell proliferation was evident in both groups because of the higher numbers of viable cells compared with day 0 (p < 0.001). These results indicate that a large number of cells remain viable and continue to proliferate after acoustofluidic treatment.

DISCUSSION

Acoustofluidics is a rapidly developing field with a broad range of applications such as particle/cell manipulation and separation (Bruus et al. 2011; Gedge and Hill 2012; Lenshof et al. 2012; Wu et al. 2017). More recently, acoustofluidic-mediated delivery has generated significant interest (Belling et al. 2020; Centner et al. 2020, 2021a, 2021b; Salari et al. 2021). However, acoustofluidic-mediated molecular delivery to cells has not been directly compared with static ultrasound systems.

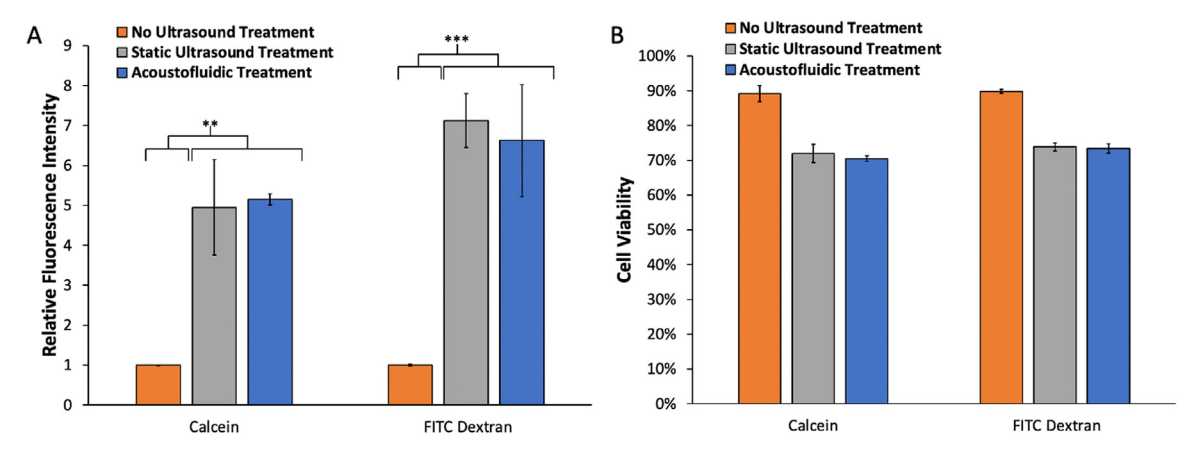


Fig. 10. (a) Delivery efficacy using $0.6~\mu g/mL$ (1 mM) of calcein (0.6~kDa) and $150~\mu g/mL$ (1 mM) of 150-kDa fluorescein isothiocyanate (FITC)—dextran was assessed with refined static treatment (5.1 MPa, 45 s and 94 $\mu g/mL$ microbubble concentration) and acoustofluidic treatment (5.1 MPa, 24 $\mu g/mL$ microbubble concentration) parameters. Static treatment and acoustofluidic treatment enhanced biomolecular delivery of calcein (ANOVA p < 0.01, n = 5 or 6/group) and 150-kDa FITC-dextran (p < 0.001) compared with negative control (no ultrasound treatment), respectively. (b) Static and acoustofluidic treatments had decreased cell viability compared with negative control (p < 0.001). No statistically significant differences in cell viability were detected between static and acoustofluidic treatments for calcein and 150-kDa FITC—dextran treatment groups, respectively (p > 0.05).

In this study, a 3-D-printed concentric spiral acoustofluidic system was tested in comparison with a static ultrasound system using the same P4-1 ultrasound transducer array. The impact of various treatment conditions on intracellular molecular delivery was evaluated in each ultrasound treatment system. Intracellular delivery of small molecules (0.6-kDa calcein) and large molecules (150-kDa FITC—dextran) was assessed in each system. Intracellular delivery of large molecules, such as CRISPR endonucleases and proteins, is of clinical significance because they have the capacity to modulate

protein expression, induce genome editing, alter cell behavior and inhibit or enhance interactions in desired cells, such as T lymphocytes, for immune therapies, gene correction and cell/tissue engineering (Cho et al. 2013; Ebina et al. 2013; Barrangou and Doudna 2016; Lee et al. 2019). One hundred fifty—kilodalton FITC—dextran is similar in molecular weight to CRISPR endonucleases, which are promising techniques for genomic modification with high specificity (Kocak et al. 2019). Additionally, 150-kDa FITC-dextran has a larger molecular weight than most mammalian proteins. For

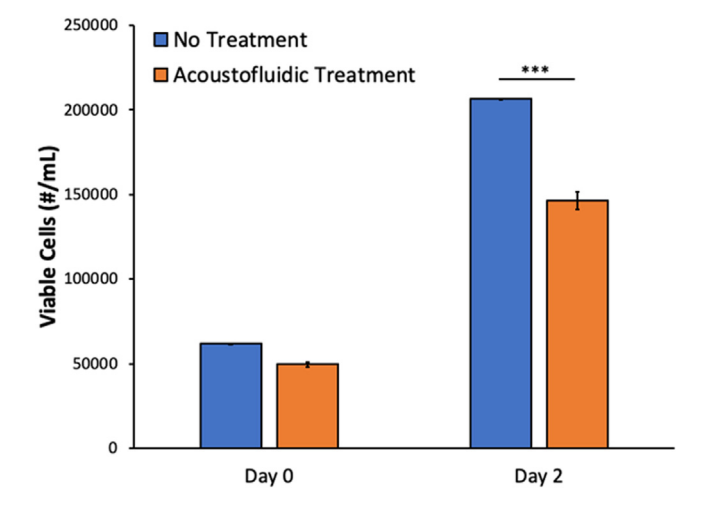


Fig. 11. Cell viability and proliferation after acoustofluidic treatment, as measured with trypan blue assay. Immediately after treatment (day 0), the number of viable cells did not statistically differ between acoustofluidic treatment and the flow-only control group (analysis of variance [ANOVA] p > 0.05, n = 5/group). At 2 days after treatment, the number of viable cells was higher in the flow-only control group compared with the acoustofluidic treatment group (p < 0.001), but cell proliferation was evident by the larger numbers of viable cells in both groups compared with day 0 (p < 0.001).

example, hemoglobin, a proteinaceous macromolecule in red blood cells that carries oxygen to tissue, has a molecular weight of approximately 65 kDa (Billett 1990). Thus, our findings provide important insights into molecular delivery of large molecules in acoustofluidic systems, relative to a traditionally used static configuration.

Previous acoustofluidic applications for molecular delivery have generally used polydimethylsiloxane (PDMS)-based photolithography techniques or a glass substrate to generate acoustofluidic devices (Belling et al. 2020; Centner et al. 2020, 2021a, 2021b; Salari et al. 2021). PDMS-Based acoustofluidic devices offer distinct advantages, such as rapid device generation and the ability to produce very small channel dimensions. However, PDMS-based acoustofluidic devices have important limitations because PDMS can have batch-to-batch variability in geometric dimensions, which can alter the ultrasound field in the acoustofluidic channel for each batch of devices (Hill et al. 2002). This can have a significant impact on reproducibility for applications such as particle/cell sorting, enrichment and molecular delivery (Hill et al. 2002, Johansson et al. 2009; Centner et al. 2020, 2021a, 2021b). Glass substrate-based acoustofluidic devices allow certain molecules and cells to adhere to the channel walls (Belling et al. 2020; Salari et al. 2021). T lymphocytes, however, are anchorage independent, and tethering biomolecules to a capillary wall may severely reduce processing rate, which can limit the availability of essential therapies. The processing rate is fundamentally important for T-lymphocyte therapies, such as CAR T, which often require approximately 10⁸ cells for each treatment (Neelapu et al. 2017; Maude et al. 2018; Schuster et al. 2019). To address these limitations, a 3-D-printed plastic-based concentric spiral acoustofluidic device allows consistent fabrication of acoustofluidic devices with consistent channel and device dimensions, which can increase reproducibility and consistency for acoustofluidic applications.

Unique to our acoustofluidic delivery technique is the utilization of microbubbles as a mediator of molecular delivery. Other studies have focused on other effects of ultrasound, such as acoustic radiation forces and microstreaming effects, where ultrasound is applied continuously to induce these effects (Belling et al. 2020; Salari et al. 2021). Acoustic radiation force has been used to force cells to the distal portion of the channel, where cells shear against the wall for enhanced molecular delivery (Belling et al. 2020). With our acoustofluidic configuration, acoustic radiation force is not expected to force cells to pressure nodes and antinodes, as a short pulse (less than 1% duty cycle) was used in this study instead of continuous ultrasound. Additionally, thermal effects are not expected to play an important role in molecular delivery because of the low duty cycle (<1%) and short exposure time ($\sim 2-3$ s) of our acoustofluidic device (Centner et al. 2021a, 2021b). However, acoustic radiation force may still potentially play a role in delivery as microbubbles can be forced radially toward cells even with short ultrasound pulse durations (Zhou et al. 2012). Microbubble destruction resulting from cavitation has been reported to induce temporary pores in the plasma membrane for effective sonoporation (Zhou et al. 2012; Hu et al. 2013). Additionally, microstreaming is induced by microbubble oscillation/cavitation and may contribute to molecular delivery (Marmottant and Hilgenfeldt 2003; Collis et al. 2010). Although the in situ acoustofluidic pressures within the channels have not been directly measured, it is feasible that microbubble oscillation/cavitation may be a predominant mechanism as our ultrasound output pressure is significantly above the stable/inertial cavitation threshold for lipid-coated microbubbles (Helfield et al. 2016). These effects could potentially facilitate molecular delivery via sonoporation, but further research is required to determine predominant mechanisms.

In this study, acoustic attenuation was measured to assess the correlation between microbubble destruction and molecular delivery. In the static configuration, reduced microbubble attenuation relative to the control group was positively correlated with increased molecular delivery ($R^2 = 0.91$). This is consistent with prior studies that observed reduced microbubble attenuation with increased ultrasound treatment time in a static configuration (Escoffre et al. 2013). Interestingly, a similar trend was not observed with acoustofluidic treatment $(R^2 = 0.00)$, indicating that there was no linear relationship between microbubble attenuation and molecular delivery. With the acoustofluidic device, a microbubble concentration of 24 μ g/mL enhanced molecular delivery to Jurkat T lymphocytes compared with all other microbubble concentrations tested with the acoustofluidic device. We previously reported a similar trend with acoustofluidic delivery in erythrocytes (Centner et al. 2020). A possible explanation for this effect is that microbubble higher concentrations can induce "shadowing" effects because of increased scattering and attenuation of ultrasound waves through microbubble solutions, resulting in reduced ultrasound pressures in more distal locations. The residence time in the 1-mm concentric spiral acoustofluidic channel is significantly shorter (\sim 2-3 s) than the 45-s treatment duration in the static configuration. Thus, there is an optimal "therapeutic window" for microbubble concentration that will enhance molecular delivery to cells with the selected acoustofluidic parameters.

The effect of ultrasound output pressure on molecular delivery has been previously described using a static ultrasound setup (Bhutto et al. 2018); however, few

studies have used cationic microbubbles for molecular delivery to T lymphocytes, which express anionic glycoproteins and glycolipids on the plasma membrane surface (Springer 1990). Cationic microbubbles may have increased affinity to the plasma membrane because of charge—charge interactions, and it has been reported that cationic microbubbles induce increased molecular delivery levels to T lymphocytes compared with neutral microbubbles when undergoing ultrasound treatment (Centner et al. 2021a, 2021b). Similar trends were observed with static treatment and acoustofluidic treatment, as both conditions had a general increase in molecular delivery at higher ultrasound output pressures (>3.8 MPa).

Ultrasound treatment duration was also investigated in the static treatment configuration and the acoustofluidic system. An increase in molecular delivery was observed with static treatment until 45 s, with no differences detected between 45 and 60 s. Yet, static treatment had similar acoustic attenuation for ultrasound durations of 30-60 s. It is possible that the microbubble lipid shell may rupture within 30 s but cavitation activity may continue for a longer duration. Without an intact lipid shell, the perfluorocarbon gas molecules may rapidly dissolve into the liquid medium before acoustic attenuation measurements are acquired (Sarkar et al. 2009). Unlike static treatment, acoustofluidic treatment did not result in a statistically significant difference in molecular delivery when comparing acoustofluidic treatment with one pass and two passes through the device (p > 0.05), suggesting that repeated exposure does not enhance molecular delivery. We previously determined that residence time within the acoustofluidic device can influence molecular delivery (Centner et al. 2020), but the parameters in the earlier study were significantly different (slower flow rate, lower ultrasound pressure, different channel dimensions and different cell type). In this study, it is possible that the amount of microbubble destruction that occurred during the first pass caused maximum levels of molecular delivery, which was not further enhanced during the second pass through the acoustofluidic device.

Refined static treatment and refined acoustofluidic treatment enhanced molecular delivery for calcein (p < 0.01) and FITC-dextran (p < 0.001) compared with respective negative control groups without acoustofluidic treatment. No statistically significant differences were detected between static treatment and acoustofluidic treatment regardless of molecular size, indicating that similar levels of molecular delivery were achieved with each configuration. Although the levels of molecular delivery were similar between configurations, the acoustofluidic system offers distinct advantages compared with static treatment, especially for anchorage-independent cells such as T lymphocytes. Static

treatment is labor intensive, has limited throughput and has increased risk of variability between batches, whereas the acoustofluidic system enables a faster processing rate, less treatment time and a lower microbubble concentration compared with static treatment while achieving similar levels of molecular delivery with small and large molecules. Future integration of a single-element transducer within a 3-D-printed fluidic chamber with preprogrammed acoustic settings will enable nonspecialized personnel to easily operate this device in a closed-flow system to maintain a sterile environment. Increased cell concentration, increased flow rate and parallelization are feasible options to further improve scalability for cell manufacturing applications. Our findings in this study represent an early step toward development of optimized methods for molecular delivery of exogenous macromolecules for potential T-lymphocyte therapies, such as CAR T.

CONCLUSIONS

This study indicates that microbubble concentration and ultrasound pressure are key factors in optimizing molecular delivery to T lymphocytes using static ultrasound systems or acoustofluidic systems. Additionally, ultrasound treatment duration was a significant factor in delivery efficiency using the static ultrasound system. Similar levels of molecular delivery were achieved for small and large molecules with refined parameters in each system, yet acoustofluidic treatment required a duration of only $\sim 2-3$ s and a 24 μ g/mL microbubble concentration for optimal delivery, whereas static ultrasound treatment required a duration of 45 s and a 94 μ g/ mL microbubble concentration. These results indicate that acoustofluidic treatment is an effective approach to intracellular delivery of biomolecules and offers distinct advantages for cell manufacturing applications. Further development of this technology could potentially improve manufacturing processes for cell-based therapies such as CAR T, which may expand treatment availability and improve patient outcomes.

Acknowledgments—This research was funded by a National Science Foundation Partnership for Innovation grant (award 1827521). The Flow Cytometry Core at the University of Louisville Christina Lee Brown Envirome Institute and Mariah Priddy provided technical assistance

Conflict of interest disclosure—J.A.K. is a co-inventor of intellectual property related to this research.

REFERENCES

Annesley CE, Summers C, Ceppi F, Gardner RA. The evolution and future of CAR T cells for B-cell acute lymphoblastic leukemia. Clin Pharmacol Ther 2018;103:591–598.

Barnkob R, Bruus H. Acoustofluidics: Theory and simulation of radiation forces at ultrasound resonances in microfluidic devices. Proc Mtgs Acoust 2009;6 020001.

- Barrangou R, Doudna JA. Applications of CRISPR technologies in research and beyond. Nat Biotechnol 2016;34:933–941.
- Belling JN, Heidenreich LK, Tian Z, Mendoza AM, Chiou TT, Gong Y, Chen NY, Young TD, Wattanatorn N, Park JH, Scarabelli L, Chiang N, Takahashi J, Young SG, Stieg AZ, De Oliveira S, Huang TJ, Weiss PS, SJ Jonas. Acoustofluidic sonoporation for gene delivery to human hematopoietic stem and progenitor cells. Proc Natl Acad Sci USA 2020;117:10976–10982.
- Bhutto DF, Murphy EM, Priddy MC, Centner CC, Moore JB IV, Bolli R, Kopechek JA. Effect of molecular weight on sonoporation-mediated uptake in human cells. Ultrasound Med Biol 2018;44:2662–2672.
- Billett HH. Hemoglobin and hematocrit. In: Walker HK, Hall WD, Hurst JW, (eds). Clinical methods: The history, physical, and laboratory examinations. 3rd editionBoston: Butterworth; 1990.
- Brentjens RJ, Santos E, Nikhamin Y, Yeh R, Matsushita M, La Perle K, Quintas-Cardama A, Larson SM, Sadelain M. Genetically targeted T cells eradicate systemic acute lymphoblastic leukemia xenografts. Clin Cancer Res 2007;13:5426–5435.
- Bruus H, Dual J, Hawkes J, Hill M, Laurell T, Nilsson J, Radel S, Sadhal S, Wiklund M. Forthcoming Lab on a Chip tutorial series on acoustofluidics: Acoustofluidics—Exploiting ultrasonic standing wave forces and acoustic streaming in microfluidic systems for cell and particle manipulation. Lab Chip 2011;11:3579–3580.
- Buzhor E, Leshansky L, Blumenthal J, Barash H, Warshawsky D, Mazor Y, Shtrichman R. Cell-based therapy approaches: the hope for incurable diseases. Regen Med 2014;9:649–672.
- Carugo D, Ankrett DN, Glynne-Jones P, Capretto L, Boltryk RJ, Zhang X, Townsend PA, Hill M. Contrast agent-free sonoporation: The use of an ultrasonic standing wave microfluidic system for the delivery of pharmaceutical agents. Biomicrofluidics 2011;5:44108–4410815.
- Centner CS, Murphy EM, Priddy MC, Moore JT, Janis BR, Menze MA, DeFilippis AP, Kopechek JA. Ultrasound-induced molecular delivery to erythrocytes using a microfluidic system. Biomicrofluidics 2020;14 024114.
- Centner CS, Moore JT, Baxter ME, Long ZT, Miller JM, Kovatsenko ES, Xie B, Menze MA, Berson RE, Bates PJ, Yaddanapudi K, Kopechek JA. Acoustofluidic-mediated molecular delivery to human T cells with a three-dimensional-printed flow chamber. J Acoust Soc Am 2021;150:4534.
- Centner CS, Murphy EM, Stamp BF, Priddy MC, Moore JT, Bates PJ, Menze MA, Yaddanapudi K, Kopechek JA. Assembly and operation of an acoustofluidic device for enhanced delivery of molecular compounds to cells. J Vis Exp 2021;167:62035.
- Chicaybam L, Barcelos C, Peixoto B, Carneiro M, Limia CG, Redondo P, Lira C, Paraguassu-Braga F, Vasconcelos ZF, Barros L, Bonamino MH. An efficient electroporation protocol for the genetic modification of mammalian cells. Front Bioeng Biotechnol 2016;4:99.
- Cho SW, Kim S, Kim JM, Kim JS. Targeted genome engineering in human cells with the Cas9 RNA-guided endonuclease. Nat Biotechnol 2013;31:230–232.
- Choe JH, Watchmaker PB, Simic MS, Gilbert RD, Li AW, Krasnow NA, Downey KM, Yu W, Carrera DA, Celli A, Cho J, Briones JD, Duecker JM, Goretsky YE, Dannenfelser R, Cardarelli L, Troyanskaya O, Sidhu SS, Roybal KT, Okada H, Lim WA. SynNotch-CAR T cells overcome challenges of specificity, heterogeneity, and persistence in treating glioblastoma. Sci Transl Med 2021;13: eabe7378.
- Collis J, Manasseh R, Liovic P, Tho P, Ooi A, Petkovic-Duran K, Zhu Y. Cavitation microstreaming and stress fields created by microbubbles. Ultrasonics 2010;50:273–279.
- Davila ML, Riviere I, Wang X, Bartido S, Park J, Curran K, Chung SS, Stefanski J, Borquez-Ojeda O, Olszewska M, Qu J, Wasielewska T, He Q, Fink M, Shinglot H, Youssif M, Satter M, Wang Y, Hosey J, Quintanilla H, Halton E, Bernal Y, Bouhassira DC, Arcila ME, Gonen M, Roboz GJ, Maslak P, Douer D, Frattini MG, Giralt S, Sadelain M, Brentjens R. Efficacy and toxicity management of 19-28z CAR T cell therapy in B cell acute lymphoblastic leukemia. Sci Transl Med 2014;6 224ra25.

- Deeks SG, Wagner B, Anton PA, Mitsuyasu RT, Scadden DT, Huang C, Macken C, Richman DD, Christopherson C, June CH, Lazar R, Broad DF, Jalali S, Hege KM. A phase II randomized study of HIV-specific T-cell gene therapy in subjects with undetectable plasma viremia on combination antiretroviral therapy. Mol Ther 2002;5:788–797.
- Dewitte H, Van Lint S, Heirman C, Thielemans K, De Smedt SC, Breckpot K, Lentacker I. The potential of antigen and TriMix sono-poration using mRNA-loaded microbubbles for ultrasound-triggered cancer immunotherapy. J Control Release 2014;194:28–36.
- DiTommaso T, Cole JM, Cassereau L, Bugge JA, Hanson JLS, Bridgen DT, Stokes BD, Loughhead SM, Beutel BA, Gilbert JB, Nussbaum K, Sorrentino A, Toggweiler J, Schmidt T, Gyuelveszi G, Bernstein H, Sharei A. Cell engineering with microfluidic squeezing preserves functionality of primary immune cells in vivo. Proc Natl Acad Sci USA 2018;115:E10907–E10914.
- Dressaire E, Sauret A. Clogging of microfluidic systems. Soft Matter 2016;13:37–48.
- Ebina H, Misawa N, Kanemura Y, Koyanagi Y. Harnessing the CRISPR/Cas9 system to disrupt latent HIV-1 provirus. Sci Rep 2013;3:2510.
- Escoffre JM, Novell A, Piron J, Zeghimi A, Doinikov A, Bouakaz A. Microbubble attenuation and destruction: Are they involved in sonoporation efficiency?. IEEE Trans Ultrason Ferroelectr Freq Control 2013;60:46–52.
- Fan Z, Liu H, Mayer M, Deng CX. Spatiotemporally controlled single cell sonoporation. Proc Natl Acad Sci USA 2012;109:16486– 16491.
- Gardner RA, Finney O, Annesley C, Brakke H, Summers C, Leger K, Bleakley M, Brown C, Mgebroff S, Kelly-Spratt KS, Hoglund V, Lindgren C, Oron AP, Li D, Riddell SR, Park JR, Jensen MC. Intent-to-treat leukemia remission by CD19 CAR T cells of defined formulation and dose in children and young adults. Blood 2017;129:3322–3331.
- Gedge M, Hill M. Acoustofluidics 17: Theory and applications of surface acoustic wave devices for particle manipulation. Lab Chip 2012;12:2998–3007.
- Hashimoto M, Takemoto T. Electroporation enables the efficient mRNA delivery into the mouse zygotes and facilitates CRISPR/ Cas9-based genome editing. Sci Rep 2015;5:11315.
- Helfield B, Black JJ, Qin B, Pacella J, Chen X, Villanueva FS. Fluid viscosity affects the fragmentation and inertial cavitation threshold of lipid-encapsulated microbubbles. Ultrasound Med Biol 2016;42:782–794.
- Hill M, Shen Y, Hawkes JJ. Modelling of layered resonators for ultrasonic separation. Ultrasonics 2002;40:385–392.
- Hu Y, Wan JM, Yu AC. Membrane perforation and recovery dynamics in microbubble-mediated sonoporation. Ultrasound Med Biol 2013;39:2393–2405.
- Janis BR, Priddy MC, Otto MR, Kopechek JA, Menze MA. Sonoporation enables high-throughput loading of trehalose into red blood cells. Cryobiology 2021;98:73–79.
- Johansson L, Nikolajeff F, Johansson S, Thorslund S. On-chip fluorescence-activated cell sorting by an integrated miniaturized ultrasonic transducer. Anal Chem 2009;81:5188–5196.
- Kawai T, Akira S. The role of pattern-recognition receptors in innate immunity: Update on Toll-like receptors. Nat Immunol 2010;11:373–384.
- Kim M, Bayly PV, Meacham JM. Motile cells as probes for characterizing acoustofluidic devices. Lab Chip 2021;21:521–533.
- Kocak DD, Josephs EA, Bhandarkar V, Adkar SS, Kwon JB, Gersbach CA. Increasing the specificity of CRISPR systems with engineered RNA secondary structures. Nat Biotechnol 2019;37:657–666.
- Kopechek JA, Haworth KJ, Raymond JL, Douglas Mast T, Perrin SR, Klegerman ME, Huang S, Porter TM, McPherson DD, Holland CK. Acoustic characterization of echogenic liposomes: Frequencydependent attenuation and backscatter. J Acoust Soc Am 2011;130:3472–3481.
- Kopechek JA, Carson AR, McTiernan CF, Chen X, Hasjim B, Lavery L, Sen M, Grandis JR, Villanueva FS. Ultrasound targeted microbubble destruction-mediated delivery of a transcription factor

- decoy inhibits STAT3 signaling and tumor growth. Theranostics 2015;5:1378–1387.
- Kopechek JA, McTiernan CF, Chen X, Zhu J, Mburu M, Feroze R, Whitehurst DA, Lavery L, Cyriac J, Villanueva FS. Ultrasound and microbubble-targeted delivery of a microRNA inhibitor to the heart suppresses cardiac hypertrophy and preserves cardiac function. Theranostics 2019;9:7088–7098.
- Lee YW, Luther DC, Kretzmann JA, Burden A, Jeon T, Zhai S, Rotello VM. Protein delivery into the cell cytosol using non-viral nanocarriers. Theranostics 2019;9:3280–3292.
- Lenshof A, Magnusson C, Laurell T. Acoustofluidics 8: Applications of acoustophoresis in continuous flow microsystems. Lab Chip 2012;12:1210–1223.
- Longsine-Parker W, Wang H, Koo C, Kim J, Kim B, Jayaraman A, Han A. Microfluidic electro-sonoporation: A multi-modal cell poration methodology through simultaneous application of electric field and ultrasonic wave. Lab Chip 2013;13:2144–2152.
- Marmottant P, Hilgenfeldt S. Controlled vesicle deformation and lysis by single oscillating bubbles. Nature 2003;423:153–156.
- Maude SL, Laetsch TW, Buechner J, Rives S, Boyer M, Bittencourt H, Bader P, Verneris MR, Stefanski HE, Myers GD, Qayed M, De Moerloose B, Hiramatsu H, Schlis K, Davis KL, Martin PL, Nemecek ER, Yanik GA, Peters C, Baruchel A, Boissel N, Mechinaud F, Balduzzi A, Krueger J, June CH, Levine BL, Wood P, Taran T, Leung M, Mueller KT, Zhang Y, Sen K, Lebwohl D, Pulsipher MA, Grupp SA. Tisagenlecleucel in children and young adults with B-cell lymphoblastic leukemia. N Engl J Med 2018;378:439–448.
- Miller DL, Bao S, Morris JE. Sonoporation of cultured cells in the rotating tube exposure system. Ultrasound Med Biol 1999;25:143–149.
- Nayerossadat N, Maedeh T, Ali PA. Viral and nonviral delivery systems for gene delivery. Adv Biomed Res 2012;1:27.
- Neelapu SS, Locke FL, Bartlett NL, Lekakis LJ, Miklos DB, Jacobson CA, Braunschweig I, Oluwole OO, Siddiqi T, Lin Y, Timmerman JM, Stiff PJ, Friedberg JW, Flinn IW, Goy A, Hill BT, Smith MR, Deol A, Farooq U, McSweeney P, Munoz J, Avivi I, Castro JE, Westin JR, Chavez JC, Ghobadi A, Komanduri KV, Levy R, Jacobsen ED, Witzig TE, Reagan P, Bot A, Rossi J, Navale L, Jiang Y, Aycock J, Elias M, Chang D, Wiezorek J, Go WY. Axicabtagene ciloleucel CAR T-cell therapy in refractory large B-cell lymphoma. N Engl J Med 2017;377:2531–2544.
- Prel A, Caval V, Gayon R, Ravassard P, Duthoit C, Payen E, Maouche-Chretien L, Creneguy A, Nguyen TH, Martin N, Piver E, Sevrain R, Lamouroux L, Leboulch P, Deschaseaux F, Bouille P, Sensebe L, Pages JC. Highly efficient in vitro and in vivo delivery of functional RNAs using new versatile MS2-chimeric retrovirus-like particles. Mol Ther Methods Clin Dev 2015;2:15039.
- Salari A, Appak-Baskoy S, Coe IR, Abousawan J, Antonescu CN, Tsai SSH, Kolios MC. Dosage-controlled intracellular delivery mediated by acoustofluidics for lab on a chip applications. Lab Chip 2021;21:1788–1797.

- Sarkar K, Katiyar A, Jain P. Growth and dissolution of an encapsulated contrast microbubble: Effects of encapsulation permeability. Ultrasound Med Biol 2009;35:1385–1396.
- Schuster SJ, Svoboda J, Chong EA, Nasta SD, Mato AR, Anak O, Brogdon JL, Pruteanu-Malinici I, Bhoj V, Landsburg D, Wasik M, Levine BL, Lacey SF, Melenhorst JJ, Porter DL, June CH. Chimeric antigen receptor t cells in refractory B-cell lymphomas. N Engl J Med 2017;377:2545–2554.
- Schuster SJ, Bishop MR, Tam CS, Waller EK, Borchmann P, McGuirk JP, Jager U, Jaglowski S, Andreadis C, Westin JR, Fleury I, Bachanova V, Foley SR, Ho PJ, Mielke S, Magenau JM, Holte H, Pantano S, Pacaud LB, Awasthi R, Chu J, Anak O, Salles G, Maziarz RT, Investigators J. Tisagenlecleucel in adult relapsed or refractory diffuse large B-cell lymphoma. N Engl J Med 2019;380:45–56.
- Sharei A, Zoldan J, Adamo A, Sim WY, Cho N, Jackson E, Mao S, Schneider S, Han MJ, Lytton-Jean A, Basto PA, Jhunjhunwala S, Lee J, Heller DA, Kang JW, Hartoularos GC, Kim KS, Anderson DG, Langer R, Jensen KF. A vector-free microfluidic platform for intracellular delivery. Proc Natl Acad Sci USA 2013;110:2082–2087.
- Springer TA. Adhesion receptors of the immune system. Nature 1990;346:425–434.
- Stoiber S, Cadilha BL, Benmebarek MR, Lesch S, Endres S, Kobold S. Limitations in the design of chimeric antigen receptors for cancer therapy. Cells 2019;8:472.
- Sugar IP, Neumann E. Stochastic model for electric field-induced membrane pores: Electroporation. Biophys Chem 1984;19:211–225
- Turtle CJ, Hanafi LA, Berger C, Gooley TA, Cherian S, Hudecek M, Sommermeyer D, Melville K, Pender B, Budiarto TM, Robinson E, Steevens NN, Chaney C, Soma L, Chen X, Yeung C, Wood B, Li D, Cao J, Heimfeld S, Jensen MC, Riddell SR, Maloney DG. CD19 CAR-T cells of defined CD4⁺:CD8⁺ composition in adult B cell ALL patients. J Clin Invest 2016;126:2123–2138.
- Wu M, Ouyang Y, Wang Z, Zhang R, Huang PH, Chen C, Li H, Li P, Quinn D, Dao M, Suresh S, Sadovsky Y, Huang TJ. Isolation of exosomes from whole blood by integrating acoustics and microfluidics. Proc Natl Acad Sci USA 2017;114:10584–10589.
- Ying Z, Huang XF, Xiang X, Liu Y, Kang X, Song Y, Guo X, Liu H, Ding N, Zhang T, Duan P, Lin Y, Zheng W, Wang X, Lin N, Tu M, Xie Y, Zhang C, Liu W, Deng L, Gao S, Ping L, Wang X, Zhou N, Zhang J, Wang Y, Lin S, Mamuti M, Yu X, Fang L, Wang S, Song H, Wang G, Jones L, Zhu J, SY Chen. A safe and potent anti-CD19 CAR T cell therapy. Nat Med 2019;25:947–953.
- Zhou Y, Shi J, Cui J, Deng CX. Effects of extracellular calcium on cell membrane resealing in sonoporation. J Control Release 2008;126:34–43.
- Zhou Y, Yang K, Cui J, Ye JY, Deng CX. Controlled permeation of cell membrane by single bubble acoustic cavitation. J Control Release 2012;157:103–111.